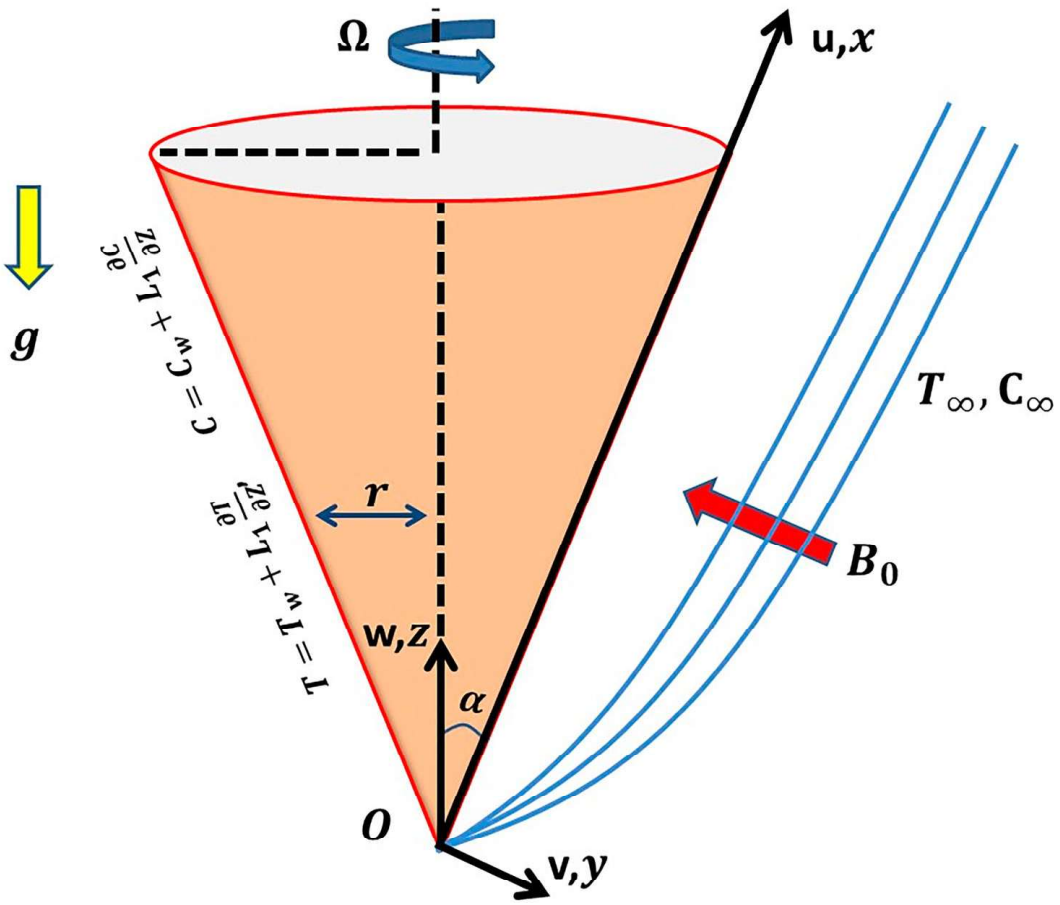

Figure 1. Geometry of the problem.

The corresponding boundary conditions are:

$$\left.\begin{aligned} At \;\; z = 0 : u = 0, v = r\Omega, T = T_w + L_1 \frac{\partial T}{\partial z}, \\ w = \frac{-D_B}{1 - C_w} \frac{\partial C}{\partial z}, C = C_w + L_2 \frac{\partial C}{\partial z} \\ As \;\; z \to \infty : u \to 0, v \to 0, T \to T_\infty, C \to C_\infty. \end{aligned}\right\} \tag{6}$$

where $r = x \sin(\alpha)$ denotes the radius of the cone, (u, v, w, T, C) denotes (velocity along x direction, velocity along y-direction, velocity along z-direction, temperature, nanoparticles volume fraction), α denotes the cone apex half-angle, B_0 denotes the intensity of the magnetic field, ρ_p denotes the density of nanoparticles, (D_B, D_T) denotes (Brownian motion diffusion factor, thermophoresis factor), $\tau = \rho_f C_{pf} / \rho_p C_{pp}$ denotes the specific heat ratio, $\rho_p C_{pp}$ denotes the specific heat of nanoparticles, L_1 and L_2 denotes the coefficients of thermal jump and nanoparticles volume fraction jump, subscripts w and ∞ denote surface of the cone and ambient state (far away from the surface).

According to Mallikarjuna et al. [44], Tien [61], Hering and Grosh [62] and Himasekhar and Sarma [63], the following similarity variables are introduced:

$$u = x\Omega \sin\alpha F(\zeta), v = x\Omega \sin\alpha G(\zeta), w = \sqrt{\nu\Omega \sin\alpha} H(\zeta)$$

$$\theta(\zeta) = \frac{T - T_\infty}{\Delta T}, \phi(\zeta) = \frac{C - C_\infty}{\Delta C}, \zeta = \sqrt{\frac{\Omega \sin\alpha}{\nu}} z \tag{7}$$

where $\Delta T = (T_w - T_\infty)\left(\frac{x}{L}\right)$ and $\Delta C = (C_w - C_\infty)\left(\frac{x}{L}\right)$ denote thermal difference and nanoparticles volume fraction difference, L denotes the slant height of the cone surface, T_w and C_w denote the cone surface temperature and NVF at the base ($x = L$). $\zeta, F, \theta, G, \phi$, and H denote similarity space variable, tangential velocity, temperature, azimuthal velocity, NVF, and normal velocity.

By the virtue of Equation (7), Equations (1)–(6) yield

$$H' = -2F \tag{8}$$

$$F'' = F'H + F^2 - G^2 + HaF - Mc\{\theta + Nc\theta^2 - Nr\phi\} \tag{9}$$

$$G'' = G'H + 2FG + HaG \tag{10}$$

$$\theta'' = \Pr(\theta'H + \theta F) - PrNb\theta'\phi' - PrNt(\theta')^2 \tag{11}$$

$$\phi'' = \mathrm{LePr}(\phi'H + \phi F) - \frac{Nt}{Nb}\theta'' \tag{12}$$

with dimensionless auxiliary conditions

$$\left.\begin{aligned} At \quad \zeta = 0 : F = 0, G = 1, H = \frac{-Sb}{LePr}\phi' \\ \theta = 1 + Ts\theta', \phi = 1 + Cs\phi' \\ As \quad \zeta \to \infty : F \to 0, G \to 0, \theta \to 0, \phi \to 0 \end{aligned}\right\} \tag{13}$$

where $Mc = \frac{Gr}{Re^2}$ denotes the mixed convection factor, $Re = \frac{\Omega L^2 \sin\alpha}{\nu}$ denotes the Reynolds number, $Gr = \frac{g\Lambda_0 \cos\alpha(1-C_\infty)(T_w - T_\infty)L^3}{\nu^2}$ denotes the Grashof number, $Nc = \frac{\Lambda_1}{\Lambda_0}\Delta T$ denotes the nonlinear convection factor, $Nr = \frac{(\rho_p - \rho_f)\Delta C}{\rho_f \Delta T \Lambda_0 (1-C_\infty)}$ denotes the buoyancy ratio, $Ha = \frac{\sigma B_0^2}{\rho_f \Omega \sin\alpha}$ denotes the Hartmann number, $Pr = \frac{\mu C_{pf}}{\kappa}$ denotes the Prandtl number, $Le = \frac{\kappa}{\rho_f C_{pf} D_B}$ denotes the Lewis number, $Nb = \frac{\tau D_B \Delta C}{\nu}$ denotes the Brownian motion number, $Nt = \frac{\tau D_T \Delta T}{T_\infty \nu}$ denotes the thermophoresis number, $Ts = L_1\sqrt{\frac{\Omega \sin\alpha}{\nu}}$ denotes the thermal slip factor, $Cs = L_2\sqrt{\frac{\Omega \sin\alpha}{\nu}}$ denotes the solutal slip factor and $Sb = \frac{\Delta C}{1-C_w}$ denotes the Stefan number.

The dimensionless Nusselt number Nur and Sherwood number Shr are given below;

$$Nur = Re^{-0.5}Nu_r = -\theta'(0) \tag{14}$$

$$Shr = Re^{-0.5}Sh_r = -\phi'(0) \tag{15}$$

3. Numerical method and validation

The nonlinear differential Equations (8)–(13) are deciphered using the shooting method featuring the Fehlberg scheme. The boundary value problem (BVP) transforms into initial value problem (IVP), to this consider the following

$$F = \mathcal{Z}_1, F' = \mathcal{Z}_2 \tag{16}$$

$$F'' = \mathcal{Z}_1^2 - \mathcal{Z}_4^2 + \mathcal{Z}_2\mathcal{Z}_3 + Ha\mathcal{Z}_1 - Mc(\mathcal{Z}_6 + Nc\mathcal{Z}_6^2 - Nr\mathcal{Z}_8) \tag{17}$$

$$H = \mathcal{Z}_3 \tag{18}$$

$$H' = -2\mathcal{Z}_1 \tag{19}$$

$$G = \mathcal{Z}_4, G' = \mathcal{Z}_5 \tag{20}$$

$$G'' = \mathcal{Z}_5\mathcal{Z}_3 + 2\mathcal{Z}_1\mathcal{Z}_4 + Ha\mathcal{Z}_4 \tag{21}$$

$$\theta = \mathcal{Z}_6, \theta' = \mathcal{Z}_7 \tag{22}$$

$$\theta'' = \Pr\{\mathcal{Z}_3\mathcal{Z}_7 + \mathcal{Z}_1\mathcal{Z}_6 - Nb\mathcal{Z}_7\mathcal{Z}_9 - Nt\mathcal{Z}_7^2\} \tag{23}$$

$$\phi = \mathcal{Z}_8, \phi' = \mathcal{Z}_9 \tag{24}$$

$$\phi'' = PrLe(\mathcal{Z}_1\mathcal{Z}_8 + \mathcal{Z}_3\mathcal{Z}_9) - \frac{PrNt}{Nb}\{\mathcal{Z}_3\mathcal{Z}_7 + \mathcal{Z}_1\mathcal{Z}_6 - Nb\mathcal{Z}_7\mathcal{Z}_9 - Nt\mathcal{Z}_7^2\} \tag{25}$$

$$\mathcal{Z}_1 = 0, \mathcal{Z}_2, \mathcal{Z}_3 + \frac{Sb}{LePr}\mathcal{Z}_9 = 0, \mathcal{Z}_4 = 1, \mathcal{Z}_5$$

$$\mathcal{Z}_6 = 1 + Ts\mathcal{Z}_7, \mathcal{Z}_7, \mathcal{Z}_8 = 1 + Cs\mathcal{Z}_9, \mathcal{Z}_9 \tag{26}$$

The above system is solved keeping the length of the domain ζ_∞ as 10, to ensure that $F(\zeta_\infty) = 0, G(\zeta_\infty) = 0, \theta(\zeta_\infty) = 0$, and $\phi(\zeta_\infty) = 0$ with accuracy of 10^{-6}. The unknown boundary conditions are determined with Newton's Raphson method, the resultant system is treated with RK-Fehlberg method.

For validation, the RK-Fehlberg scheme results are compared with those obtained by the Finite Element Method (FEM). So, by applying the variational formulation with linear element $\Omega_e = (\zeta_e, \zeta_{e+1})$, leads to

$$\begin{bmatrix} [A^{11}] & [A^{12}] & [A^{13}] & [A^{14}] & [A^{15}] \\ [A^{21}] & [A^{22}] & [A^{23}] & [A^{24}] & [A^{25}] \\ [A^{31}] & [A^{32}] & [A^{33}] & [A^{34}] & [A^{36}] \\ [A^{41}] & [A^{42}] & [A^{43}] & [A^{44}] & [A^{45}] \\ [A^{51}] & [A^{52}] & [A^{53}] & [A^{54}] & [A^{55}] \end{bmatrix} \begin{bmatrix} \{H\} \\ \{F\} \\ \{G\} \\ \{\theta\} \\ \{\phi\} \end{bmatrix} = \begin{bmatrix} \{c\}^1 \\ \{c\}^2 \\ \{c\}^3 \\ \{c\}^4 \\ \{c\}^5 \end{bmatrix}$$

where $[A^{mn}]$and $\{c\}^m (m, n = 1, .., 5)$ are defined as:

$$A_{ij}^{11} = \int_{\zeta_e}^{\zeta_{e+1}} N_i \frac{dN_j}{d\zeta} d\zeta, A_{ij}^{12} = 2\int_{\zeta_e}^{\zeta_{e+1}} N_i N_j d\zeta, A_{ij}^{13} = A_{ij}^{14} = A_{ij}^{15} = A_{ij}^{21} = 0,$$

$$A_{ij}^{22} = -\int_{\zeta_e}^{\zeta_{e+1}} \frac{dN_i}{d\zeta}\frac{dN_j}{d\zeta} d\zeta - \int_{\zeta_e}^{\zeta_{e+1}} N_i\overline{H}\frac{dN_j}{d\zeta} d\zeta - \int_{\zeta_e}^{\zeta_{e+1}} N_i\overline{F}N_j d\zeta$$

$$- Ha\int_{\zeta_e}^{\zeta_{e+1}} N_i N_j d\zeta, A_{ij}^{23} = \int_{\zeta_e}^{\zeta_{e+1}} N_i\overline{G}N_j d\zeta, A_{ij}^{24}$$

$$= Mc\int_{\zeta_e}^{\zeta_{e+1}} N_i N_j d\zeta + McNc\int_{\zeta_e}^{\zeta_{e+1}} N_i\overline{\theta}N_j d\zeta, A_{ij}^{25} = -McNr\int_{\zeta_e}^{\zeta_{e+1}} N_i N_j d\zeta,$$

$$A_{ij}^{31} = A_{ij}^{32} = 0, A_{ij}^{33} = -\int_{\zeta_e}^{\zeta_{e+1}} \frac{dN_i}{d\zeta}\frac{dN_j}{d\zeta} d\zeta - 2\int_{\zeta_e}^{\zeta_{e+1}} N_i\overline{F}N_j d\zeta - \int_{\zeta_e}^{\zeta_{e+1}} N_i\overline{H}\frac{dN_j}{d\zeta} d\zeta$$

$$- Ha\int_{\zeta_e}^{\zeta_{e+1}} N_i N_j d\zeta, A_{ij}^{34} = A_{ij}^{35} = 0,$$

Table 1. Comparison of results obtained from three different methods when $Ha = Nb = Nt = 0.2, Le = Pr = 1, Cs = Ts = Mc = Nc = Nr = 0.1$ and $Sb = 1$.

	Fehlberg method		BVP5c		FEM	
Sb	*Nur*	*Shr*	*Nur*	*Shr*	*Nur*	*Shr*
0.5	0.472037	0.285798	0.472037	0.285799	0.472037	0.285798
1	0.529425	0.283222	0.529425	0.283222	0.529425	0.283222
1.5	0.590571	0.280691	0.590571	0.280691	0.590571	0.280691
2	0.656181	0.279296	0.656182	0.279296	0.656181	0.279296
2.5	0.728343	0.280180	0.728343	0.280180	0.728343	0.280180
Ha						
0.2	0.529425	0.283222	0.529425	0.283222	0.529425	0.283222
0.4	0.489130	0.255991	0.489131	0.255992	0.489130	0.255992
0.6	0.454212	0.234084	0.454212	0.234084	0.454212	0.234084
0.8	0.424476	0.216988	0.424483	0.217041	0.424476	0.216988
1	0.399343	0.203834	0.399345	0.203848	0.399343	0.203834

$$A_{ij}^{41} = A_{ij}^{42} = A_{ij}^{43} = 0, A_{ij}^{44} = -\int_{\zeta_e}^{\zeta_{e+1}} \frac{dN_i}{d\zeta}\frac{dN_j}{d\zeta}d\zeta - Pr\int_{\zeta_e}^{\zeta_{e+1}} N_i\bar{H}\frac{dN_j}{d\zeta}d\zeta - Pr\int_{\zeta_e}^{\zeta_{e+1}} N_i\bar{F}N_j d\zeta$$
$$+ PrNt\int_{\zeta_e}^{\zeta_{e+1}} \frac{dN_i}{d\zeta}\bar{\theta}\frac{dN_j}{d\zeta}d\zeta, A_{ij}^{45} = PrNb\int_{\zeta_e}^{\zeta_{e+1}} \frac{dN_i}{d\zeta}\bar{\theta}\frac{dN_j}{d\zeta}d\zeta,$$
$$A_{ij}^{51} = A_{ij}^{52} = A_{ij}^{53} = 0, A_{ij}^{54} = -\frac{Nt}{Nb}\int_{\zeta_e}^{\zeta_{e+1}} \frac{dN_i}{d\zeta}\frac{dN_j}{d\zeta}d\zeta, A_{ij}^{55} = -\int_{\zeta_e}^{\zeta_{e+1}} \frac{dN_i}{d\zeta}\frac{dN_j}{d\zeta}d\zeta$$
$$- \Pr Le\int_{\zeta_e}^{\zeta_{e+1}} N_i\bar{H}\frac{dN_j}{d\zeta}d\zeta - \Pr Le\int_{\zeta_e}^{\zeta_{e+1}} N_i\bar{F}N_j d\zeta,$$
$$c_i^1 = 0, c_i^2 = -\left(N_i\frac{dF}{d\zeta}\right)_{\zeta_e}^{\zeta_{e+1}}, c_i^3 = -\left(N_i\frac{dG}{d\zeta}\right)_{\zeta_e}^{\zeta_{e+1}}, c_i^4 = -\left(N_i\frac{d\theta}{d\zeta}\right)_{\zeta_e}^{\zeta_{e+1}},$$
$$c_i^5 = -\left(N_i\left(\frac{d\phi}{d\zeta} + \frac{Nt}{Nb}\frac{d\theta}{d\zeta}\right)\right)_{\zeta_e}^{\zeta_{e+1}}.$$

where $\bar{\Phi} = \sum_{i=1}^{2} \overline{\Phi_i} N_i$ and $\Phi(F, G, H, \theta, \phi)$ is dependent variable and N_i is linear shape function. Linearized equations are unraveled by the Gauss elimination method with an aaccuracy 10^{-8}. Table 1 presents a very good agreement. Flow chart of both Fehlberg method and FEM is outlined in Figure 2.

4. Interpretation of results

Obtained results are analyzed and discussed in detail in this section. Results are computed for Hartmann number ($0 \leq Ha \leq 2$), mixed convection factor ($0 \leq Mc \leq 1.6$), nonlinear convection factor ($0 \leq Nc \leq 20$), Stefan Blowing number ($-2 \leq Sb \leq 2$), thermo-migration factor ($0.1 \leq Nt \leq 1.7$), Brownian motion number ($0.1 \leq Nb \leq 1.7$), thermal slip factor ($0 \leq Ts \leq 2.0$), solutal slip factor ($0.5 \leq Cs \leq 2.5$), Prandtl number ($Pr = 6$) and Lewis number ($Le = 3$). 3D surface plots and contour plots are plotted to examine the Nusselt number and Sherwood number.

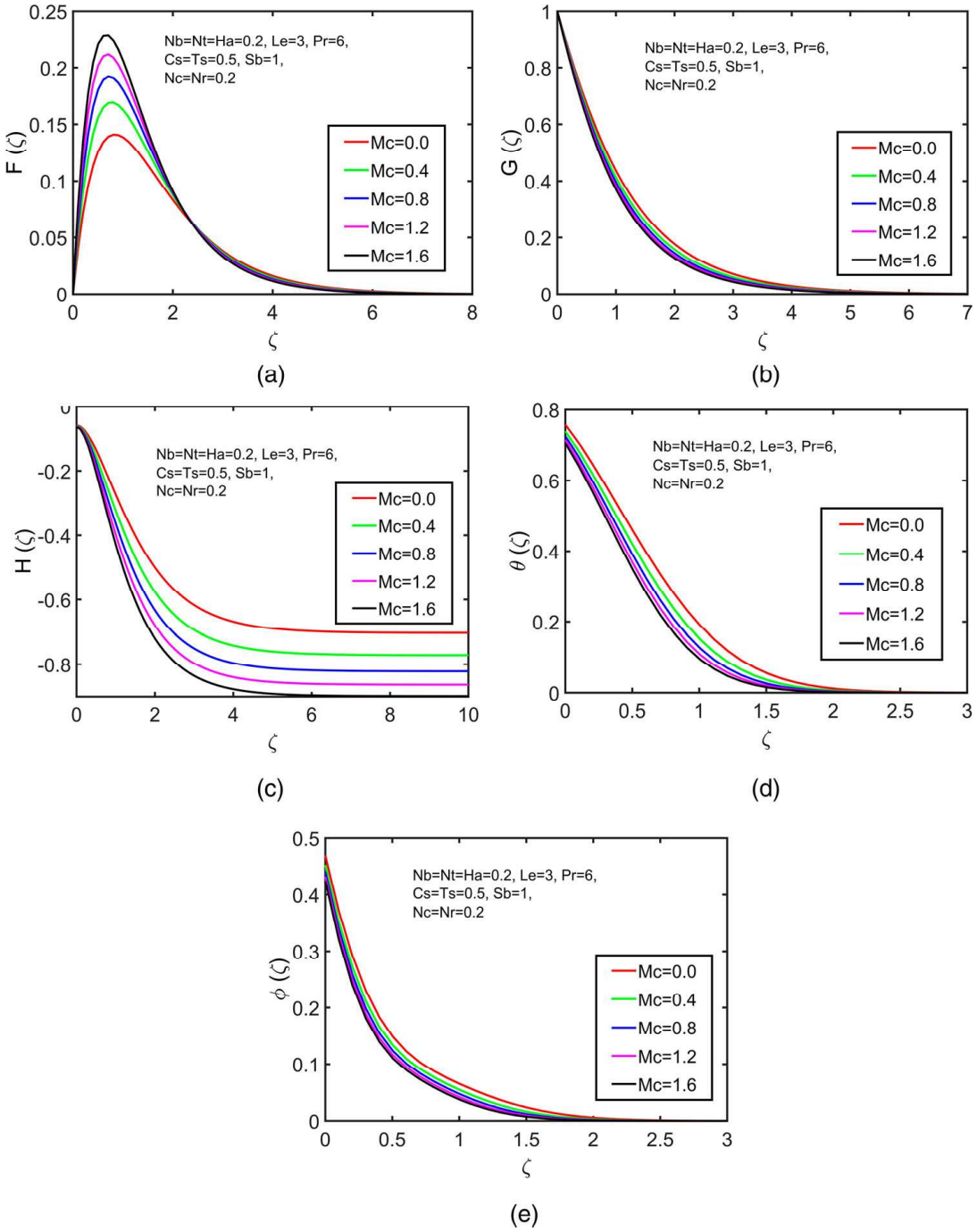

Figure 4. (a)–(e): Consequences of *Mc* on $F(\zeta)$, $G(\zeta)$, $H(\zeta)$, $\theta(\zeta)$ and $\phi(\zeta)$ respectively.

force $Mc\{\theta - Nr\phi\}$, the nonlinear convection factor *Nc* is additional to the buoyancy upright force, i.e. $Mc\{\theta + Nc\theta^2 - Nr\phi\}$. Therefore, the influences of *Mc* and *Nc* are qualitatively similar. The nonlinear convection mechanism augments the tangential velocity field and can be used to control the movement of operating liquids.

In Figure 6(a)–(d), the stimulus of Stefan blowing factor ($Sb = -2, -1, 0, 1, 2$) on $F(\zeta), H(\zeta), \theta(\zeta)$ and $\phi(\zeta)$ respectively are shown. The Stefan blowing factor can be positive or negative. $Sb > 0$ represents the evaporation process (blowing), $Sb < 0$ represents

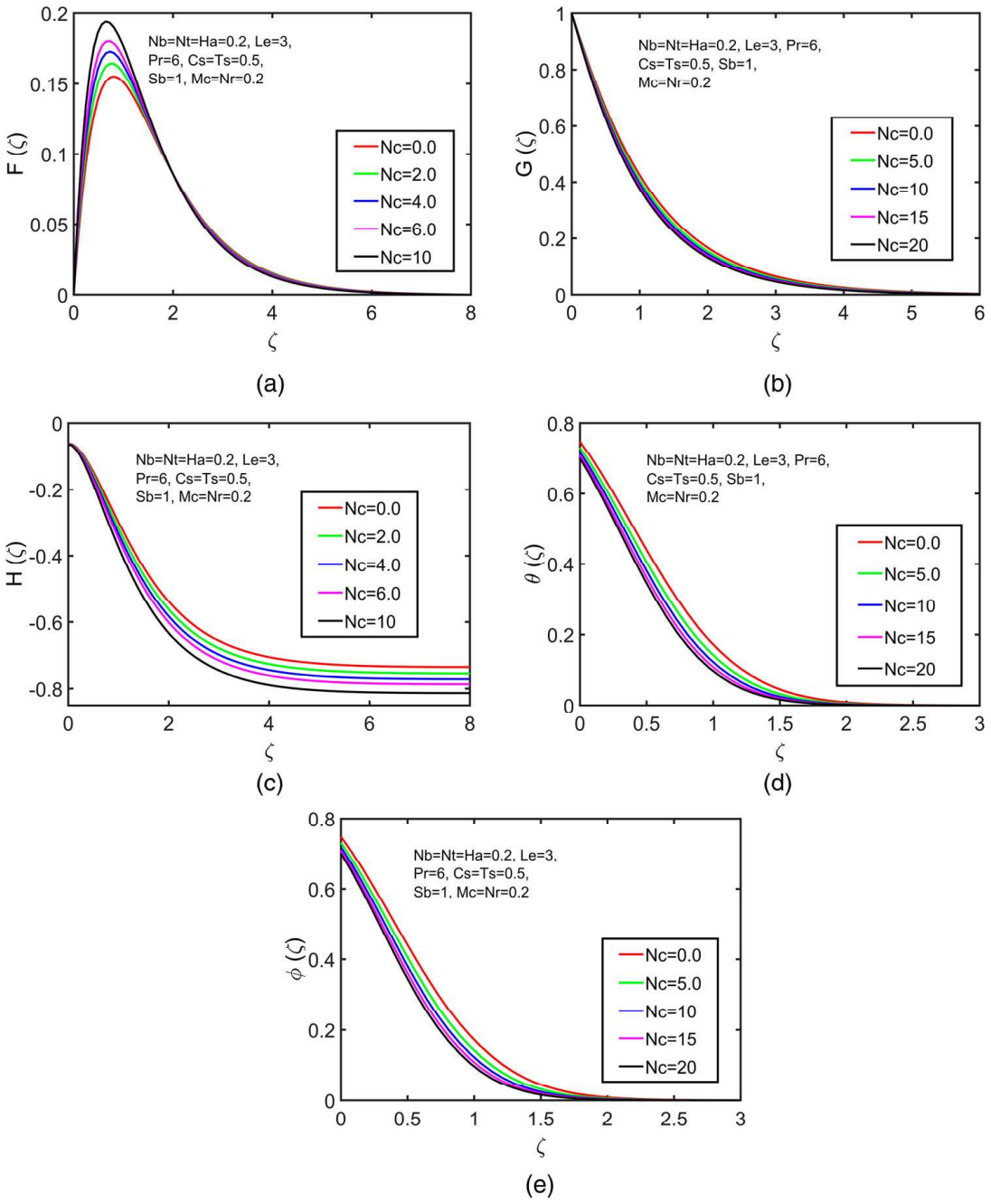

Figure 5. (a)–(d): Consequences of *Nc* on $F(\zeta)$, $G(\zeta)$, $H(\zeta)$, and $\theta(\zeta)$ respectively.

the condensation process (mass suction), and $Sb = 0$ represents the no Stefan blowing process. The evaporation process is found to reduce the velocities ($F(\zeta)$ and $H(\zeta)$). By definition of $Sb = \frac{C_w - C_\infty}{1 - C_w}$, when we say $Sb > 0$, the nanoparticles volume fraction species are transferred from the cone surface to free stream (i.e. evaporation). Reduction in the magnitude of $F(\zeta), H(\zeta), \theta(\zeta)$ and $\phi(\zeta)$ occurs for upsurging positive *Sb* values, due to an enormous diffusion of mass from the cone surface to the free stream. However, in the case of the condensation process, the magnitude of $F(\zeta), H(\zeta), \theta(\zeta)$ and $\phi(\zeta)$ increases with ascending

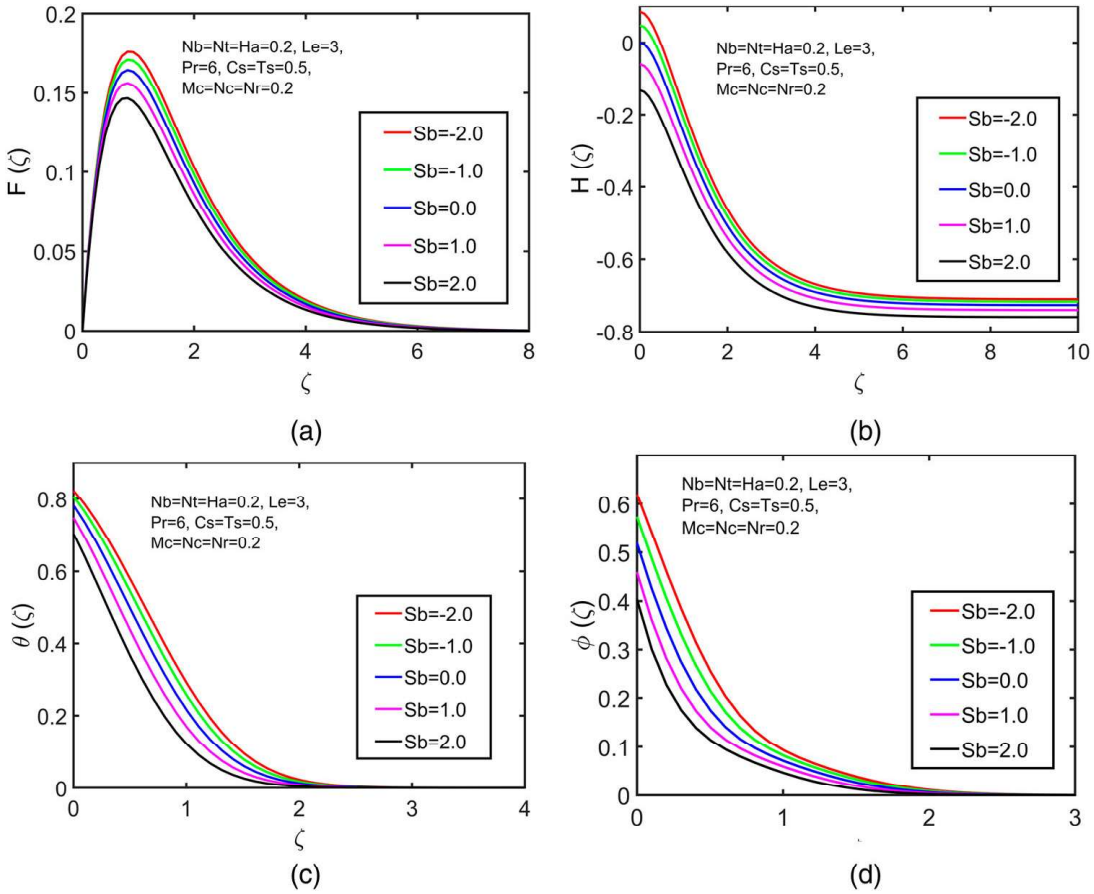

Figure 6. (a)–(d): Consequences of *Sb* on $F(\zeta)$, $H(\zeta)$, $\theta(\zeta)$ and $\phi(\zeta)$ respectively.

negative *Sb* values. Our results of the Stefan blowing process are agreed with those of Fang and Jing [46].

Figure 7(a)–(d) displays representative profiles of tangential velocity ($F(\zeta)$), normal velocity ($H(\zeta)$), temperature ($\theta(\zeta)$), and nanoparticles volume fraction ($\phi(\zeta)$) for distinct values of the thermophoretic parameter (*Nt*). An upsurge in *Nt* leads to a reduction in the magnitude of the normal velocity ($H(\zeta)$), while $F(\zeta)$, $\theta(\zeta)$, and $\phi(\zeta)$ increase with *Nt*. Since the thermophoretic factor (*Nt*) is positively associated with thermal gradient, the thermal layer thickness enlarges with *Nt*. Mathematically, since the thermophoretic term ($PrNt(\theta')^2$) occurs in the thermal energy Equation (11) with a positive sign, increasing values of *Nt* improve the thermal energy field ($\theta(\zeta)$). Similarly, the term $\frac{Nt}{Nb}\theta''$ in Equation (12) is accountable for increasing the magnitude of $\phi(\zeta)$. The enhanced thermal energy field $\theta(\zeta)$ is liable for amplification in the tangential velocity ($F(\zeta)$) for higher *Nt* (see Figure 7(a)).

The consequence of the Brownian motion number (*Nb*) on $F(\zeta)$, $H(\zeta)$, $\theta(\zeta)$ and $\phi(\zeta)$ are revealed in Figure 8(a)–(d). As expected, the thermal energy $\theta(\zeta)$ and tangential velocity $F(\zeta)$ upsurge considerably with *Nb*. But, the normal velocity ($H(\zeta)$) and nanoparticle volume fraction $\phi(\zeta)$ were condensed with upsurging values of *Nb*. The disordered movement of the nanoparticles helps to produce additional thermal energy in the liquid system and at the same time strengthens the deposition of nanoparticles outside the system, so it is responsible for condensation of $\phi(\zeta)$. Mathematically, since the Brownian term ($PrNb\theta'\phi'$) appears in the thermal energy Equation (11) with a positive sign, increasing values of *Nb*

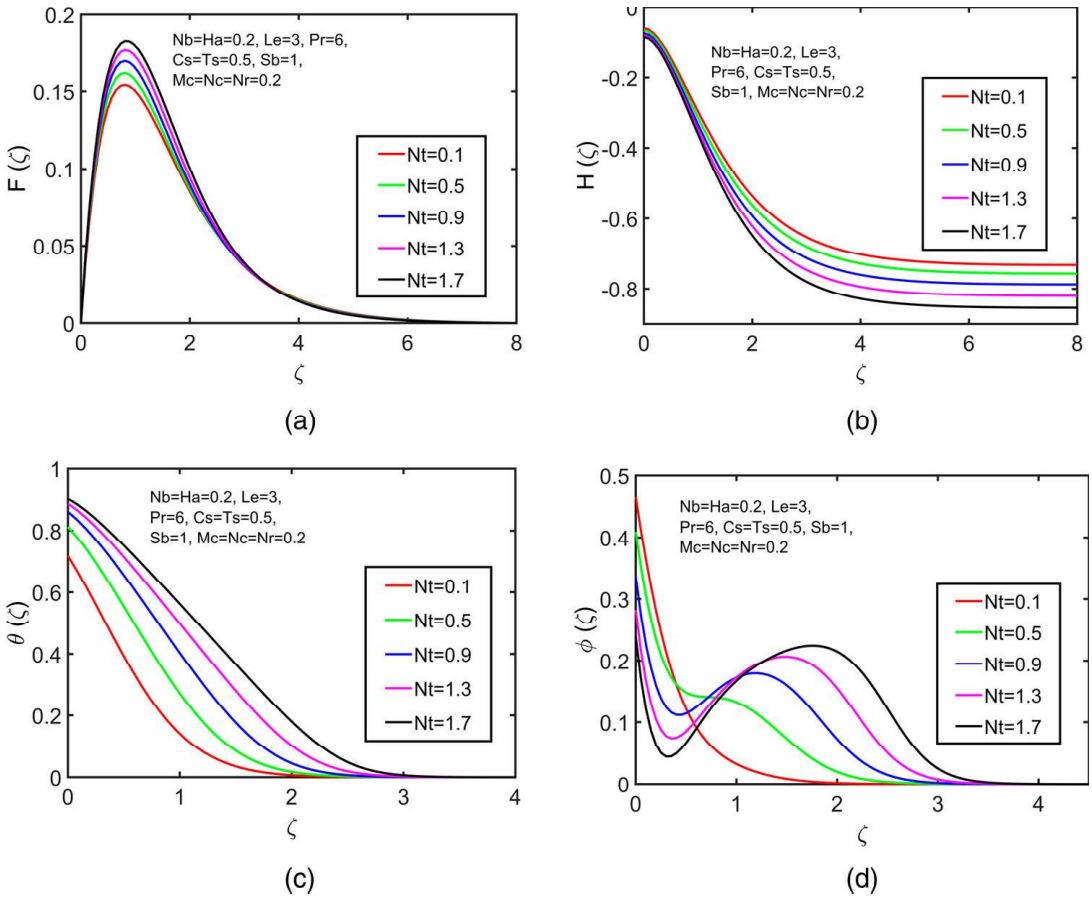

Figure 7. (a)–(d): Consequences of *Nt* on $F(\zeta)$, $H(\zeta)$, $\theta(\zeta)$ and $\phi(\zeta)$ respectively.

improve the thermal energy field ($\theta(\zeta)$). Similarly, since *Nb* occurs in the denominator of the term $\frac{Nt}{Nb}\theta''$ in Equation (12), increasing values of *Nb* reduce the magnitude of $\frac{Nt}{Nb}\theta''$ and therefore reduces $\phi(\zeta)$ considerably. The augmented $\theta(\zeta)$ and the reduced $\phi(\zeta)$ are liable for the amplification of $F(\zeta)$ for higher *Nb* through buoyancy force (see Figure 8(a)). From Figures 7 and 8 one can conclude that the influence of thermophoretic factor is stronger than Brownian number (*Nb*) on flow fields.

In Figure 9(a,b), the significance of *Ts* and *Cs* on $\theta(\zeta)$ and $\phi(\zeta)$ respectively. The thermal energy $\theta(\zeta)$ and the volumetric fraction of the nanoparticles $\phi(\zeta)$ reduce as the *Ts* and *Cs* values increase correspondingly. The nanoliquid near the cone surface skips absorbing heat energy from the cone surface. Subsequently, the thermal energy field is reduced to an increase in the *Ts* values. The effect of *Cs* on $\phi(\zeta)$ is analogous to that of *Ts* on $\theta(\zeta)$.

Figures 10–15 determine the combined effects of (*Nb*, *Nt*), (*Mc*, *Nc*), and (*Ha*, *Sb*) on Nusselt number (*Nur*) and Sherwood number (*Shr*) using 3D surface and contour graphs. Figure 10(a,b) depicts that *Nur* declines with enlarging values of both *Nb* and *Nt*, which indicates that *Nur* is at its maximum when both *Nt* and *Nb* are held at a lower magnitude. This trend exemplifies the thermal rise features of nanoliquids, as explained by several researchers [4,8,10] since a lower *Nur* indicates higher thermal energy in the liquid itself. The Sherwood number fluctuates nonlinearly through *Nb* and *Nt*, as revealed in Figure 11(a,b). The slightest *Shr* magnitude is observed when both *Nb* and *Nt* are kept minimum, but the

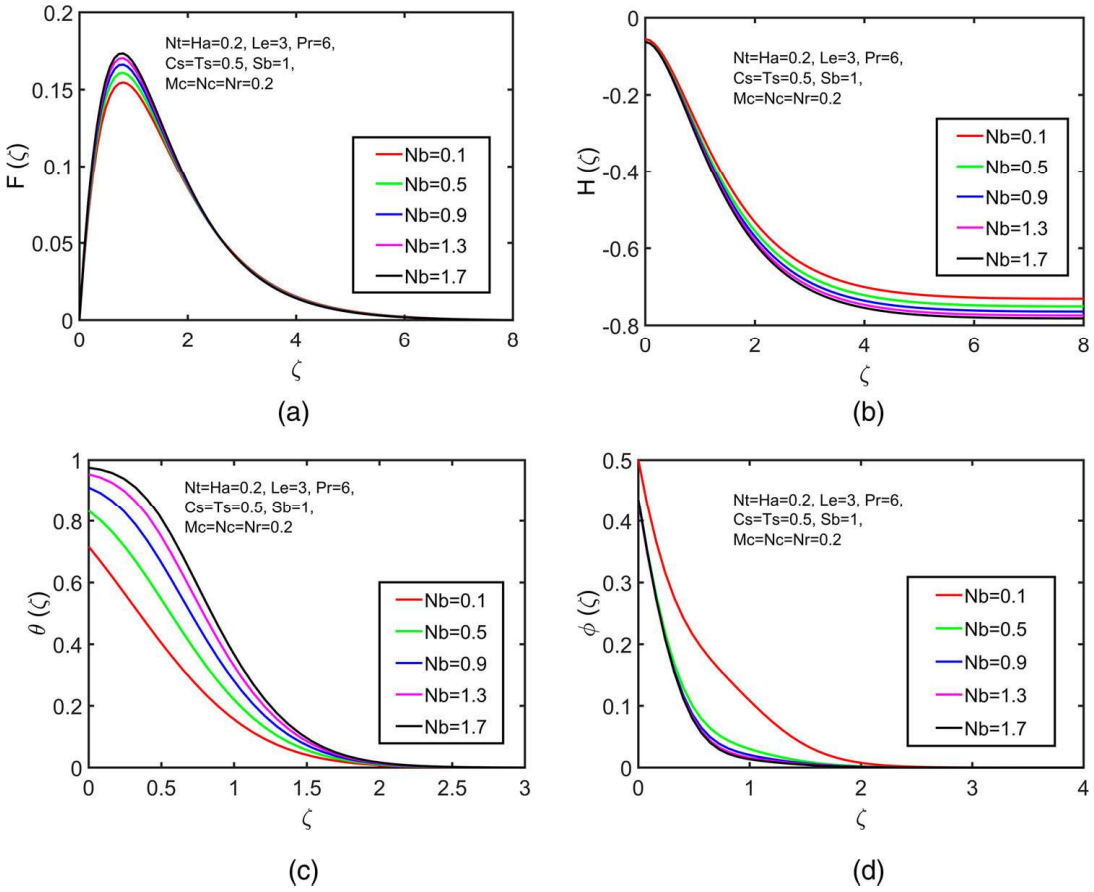

Figure 8. (a)–(d): Consequences of *Nb* on $F(\zeta), H(\zeta), \theta(\zeta)$ and $\phi(\zeta)$ respectively.

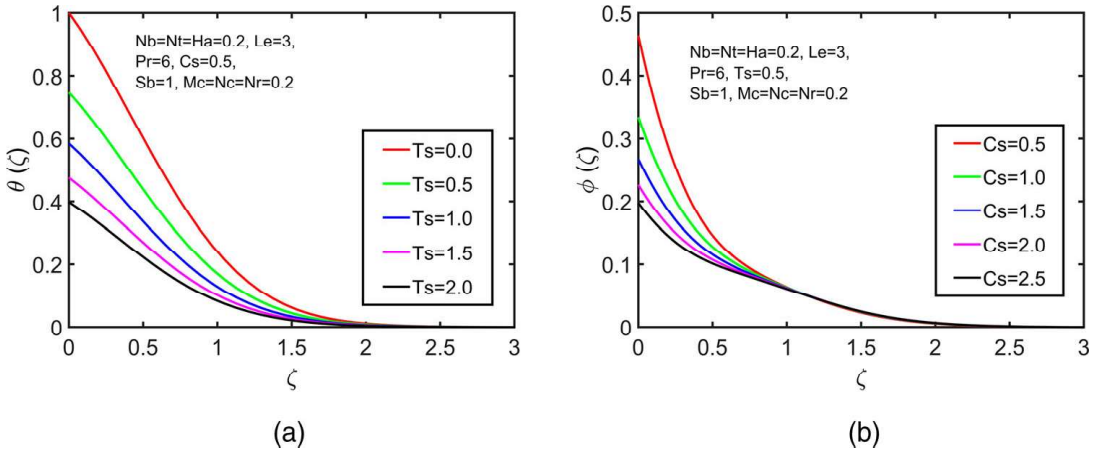

Figure 9. (a) and (b): Consequences of *Ts* and *Cs* on $\theta(\zeta)$ and $\phi(\zeta)$ respectively.

largest *Shr* is observed when *Nt* is at a high level and *Nb* is at an intermediate level. The outcomes of *Shr* relating to both *Nb* and *Nt* are consistent with Figures 7 and 8.

Figure 12(a,b) indicates that both the nonlinear convection factor (*Nc*) and the mixed convection factor (*Mc*) aid to improve the *Nur*. The maximum magnitude of *Nur* is perceived when both *Nc* and *Mc* are kept at maximum since the thermal energy layer on the surface